Orthogonal cutting of TA6V alloys with chamfered tools: Analysis of tool–chip contact lengths

Floran Barelli, Vincent Wagner, Raynald Laheurte, Gilles Dessein, Philippe Darnis, Olivier Cahuc, Michel Mousseigne

Orthogonal cutting of TA6V alloys with chamfered tools: Analysis of tool–chip contact lengths

Floran Barelli[1], Vincent Wagner[1], Raynald Laheurte[2], Gilles Dessein[1], Philippe Darnis[2], Olivier Cahuc[2] and Michel Mousseigne[3]

Abstract

In aerospace industry, the materials constituting aircraft evolved considerably in recent decades. The choice of composite materials (carbon fiber–reinforced plastic or multi-material) reduces the weight of structures, but for critical parts that support important forces or temperature, the indicated materials are alloys based on nickel or titanium. Consumption of titanium for the aerospace industry is growing rapidly, and the new generations of aircraft show an increase in the percentage of titanium. The TA6V is mostly used for structural parts, especially for engine pylon. Due to its low thermal properties, it shows a poor machinability, leading tools to undergo severe wears. The aim of this work is to understand the relation between cutting conditions and chamfered tool geometries on chip formation and tool wear. Based on a model dedicated to the understanding of cutting process with chamfered tool and on experimental tests, this work will show the influence of feed, cutting speed, chamfer length and rake angle on tool–chip contact lengths. It will also show the influence of these parameters on the variability of these contacts within a same geometry or cutting condition. This will lead to another interpretation of tool wears and pressures on the rake face.

Keywords

Turning, orthogonal cutting, chamfered tools, titanium alloy, wear, tool–chip contact length, temperatures

Introduction

In machining of annealed titanium TA6V αβ, two major tool wears can be encountered. Indeed, due to the high strength and weak thermal properties of these alloys, the tool can undergo tool breakage and diffusion wear. Tool wears in titanium alloys have been studied for a longtime.[1,2] A common solution to avoid tool breakage is to strengthen the edge by edge preparations such as a chamfer. Thus, it remains to find optimal tool geometries and cutting conditions in order to slow down or prevent diffusion wear mechanisms. Since diffusion wear mostly results from thermomechanical actions of the chip on the rake face, the understanding of tool–chip contact length can lead to a mastery of wear mechanisms.

When the tool penetrates the material, under a high pressure, a plastic strain occurs. A shear is then created at the tip of the tool, giving existence to a chip formation. This chip will flow on the rake face of the tool, leading to a specific contact between these two materials. Hence, cutting parameters as well as tool geometries impact these contacts by their influence on frictions and temperatures developed by shear and friction zones during the cutting process. General assumptions are made that the tool–chip contact length decreases with increase in cutting speed and rake angle and increases with feed.[3]

Lee and Shaffer[4] and Abdulaze[5] developed analytical tool–chip contact length models for standard steels related to geometrical aspects such as the rake angle, the uncut chip thickness and the shear angle. Zhang et al.[6] introduced the effect of cutting velocity on the prediction of these lengths and in application with low-carbon steel. Still for low-carbon steels, Oxley[7] gives a

[1]Laboratoire Génie de Production, ENIT-INPT, Université de Toulouse, Tarbes, France
[2]I2M, UMR 5295, Université de Bordeaux, Talence, France
[3]Institut Clément Ader, Université de Toulouse, Toulouse, France

Corresponding author:
Floran Barelli, Laboratoire Génie de Production, ENIT-INPT, Université de Toulouse, F-65016 Tarbes, France.
Email: floran.barelli@enit.fr

Table 1. Material constitution of TA6V (%).

	Elements (% by mass)									
	Al	V	Fe	C	D	N	H	Y	Other elements	Ti
Min.	5.5	3.5			0.12					
Max.	5.75	4.5	0.3	0.08	0.2	0.05	0.15	0.005	< 0.4	Else

model using coefficients traducing the strain hardening of the material. Many authors have developed models to predict the influence of cutting parameters and tool geometries on temperature fields in cutting zone. Lazoglu and Altintas[8] and Armarego[9] based their analysis on finite difference and Oxley[7] on slip-line field. Moufki et al.[10] attempt to take into account the dependence on temperature of the friction law between the chip and the tool, where most of the studies use a Coulomb contact. More and more models are based on the finite element method, since it can provide access to stresses, strains and temperatures in every part of the cutting zone and also predict the chip morphology.[11–13]

A major part of these models are meant for sharp edge tool modeling; however, when machining with chamfered tools, the cutting process is relatively different. Indeed, the chamfered edge will often lead to the formation of a dead metal zone under itself. This dead metal zone will replace the missing nose of the tool and form a small edge radius, changing the shear angle. With this specific shape will appear a stagnation point around which the material will flow. From this point to the cut surface, an important augmentation of speed is noted. This will generate high amount of straining around the tertiary zone[14] (located near the flank wear).

This study aims to show that the impact of cutting conditions and rake angle on cutting process and thus on tool–chip contact lengths exhibits noteworthy differences with evolutions found for perfect sharp tools. A competition between phenomena will lead to the obtaining of different temperatures and friction coefficients, depending on the chamfer geometry, rake angle and cutting conditions.[15,16] Moreover, cutting conditions and tool geometries will have an impact on chip segmentation.[17] Hence, tool–chip contact lengths will follow more complex evolutions than those usually found. From these various evolutions will result a different analysis of tool wears and tool–chip contact interactions.

In order to evaluate the impact of cutting conditions and tool geometries on apparent friction coefficients, temperatures in primary shear zone and around the chamfer, a specific experimental procedure is build. It will associate cutting forces' measurement and cutting process visualization with high-speed cameras. First, cutting forces will give shear forces as well as friction forces on the rake face. Then, the recorded images allow the identification of shear angles and tool–chip contact lengths for every step of the cutting process and for each set of cutting conditions and tool geometry. Using the analytical modeling of mechanics of machining with chamfered tools developed by Ren and Altintas[18] will provide a characterization of the influence of cutting conditions and tool geometries on the cutting process and thus on tool–chip contact lengths.

Table 2. Insert's geometries.

Inserts	Chamfer angle, α_1 (°)	Chamfer length, b_{ch} (mm)	Rake face angle, α_0 (°)
1	15	0.09252	10
2	15	0.1359	10
3	15	0.087	20
4	15	0.1676	20

Materials and methods

Experimental devices

For this study, the machining center used is Genymab 900 produced by Somab. This machining center allows the performing of milling and turning operations. For this work, conditions of orthogonal cutting are chosen by performing facing operations on tubulars of 1-mm thickness. The material chosen for this study is an annealed titanium TA6V αβ whose composition is given in Table 1.

In order to understand and analyze the influence of tool geometry and cutting conditions on chip generation and cutting forces in orthogonal cutting, several turning inserts, made of tungsten carbide, with various cutting angles and chamfered edge lengths are chosen. All the insert's geometries are summed up in Table 2, and the overall geometry is shown in Figure 1. For each insert, a set of cutting conditions is explored. Cutting condition values used are shown in Table 3.

Inserts' chamfer lengths and angles chosen are representative of common cutting edge geometries exhibited by milling tools. As well, cutting conditions have been chosen in agreement with standard values for titanium alloys and are derived from a tool material pair experimental study performed in machining by the authors. Therefore, they fulfill a design experiment (not shown in this article).

Cutting force measurements are made with a multicomponent force dynamometer Kistler 9257B, a signal

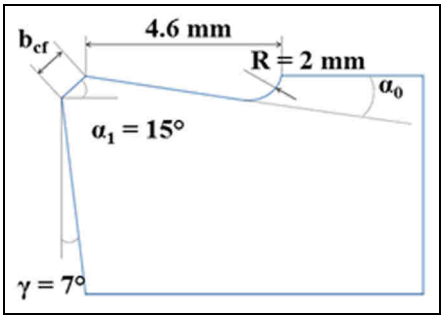

Figure 1. Insert's geometry.

Table 3. Cutting conditions.

Test	Cutting speeds ($m\,min^{-1}$)	Feed–chamfer length ratios
1	50	0.5
2	50	1
3	50	2
4	80	0.5
5	80	1
6	80	2

amplifier 5019A Kistler and the operating software DynoWare. Only forces parallel to the feed and cutting velocity are considered. Concerning the chip formation observations, a camera Photron SA1 with a high acquisition speed is used. A 3000 frames per second frequency is chosen so as to observe tool–chip contact lengths during each orthogonal cutting operation. Since the exposure time of the camera's photoelectric cell decreases as the acquisition frequency increases, this frequency allows to observe high-speed phenomena (such as chip forming) and to keep images with enough contrasts to be analyzed. The objective is placed orthogonal to the chip formation and a 100 × lens with optical rings is used to obtain the highest zoom possible in the tool–chip area. For the light, cold light spotlights are used in order to not disturb the thermal aspects of the cutting process. The complete setup is shown in Figure 2.

If forces' data are easy to exploit, images gathered by the high-speed camera need some treatment in order to measure the tool–chip contact lengths.

The image analysis is made by the realization of two major steps. One corresponds to the pretreatment of images using a free software named ImageJ.[19] The purpose of this step is to prepare the images automatically analyzed in the second step using a self-made algorithm developed on the software MATLAB.

Pretreatment on ImageJ to prepare the images

For each cutting condition and tool geometry, a set of 5000 images is obtained, thanks to the using of the high acquisition camera. In order to reduce time and

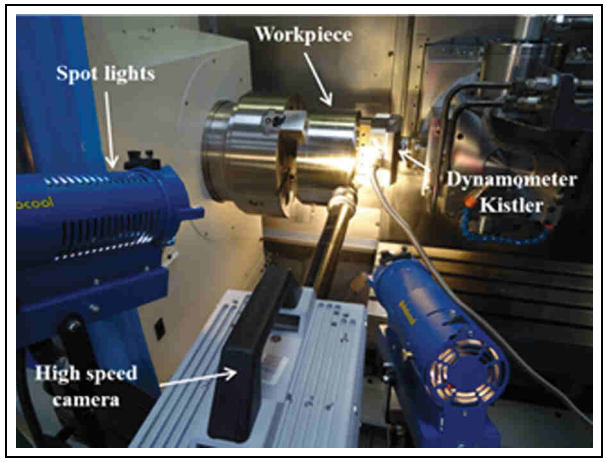

Figure 2. Experimental setup.

memory space, only 100 images for each condition are kept. The selection is made within a range of images showing stable cutting conditions (steady feed). This number of images provides enough various tool–chip contact lengths to get a rich statistical analysis.

Each set of images is in grayscale, and depending on the efficiency of the light during the experiment, it is more or less exploitable in its initial state. The first step of the pretreatment process consists of enhancing contrasts to spot the light on major elements of the image such as the tool and the chip. This step has no influence on the measurement. It just allows to process next steps in an easier way. Then, the tool is artificially set to white (grayscale of 255) and the cutting edge to black (grayscale of 0). A specific zone is also created on the left of the tool tip in order to make easier its location (black and white zones).

Post-treatment on MATLAB to determine the tool–chip contact length

The aim of the post-treatment on MATLAB is to automatically find the chip contour and calculate the tool–chip contact length for each image. Figure 3 shows main steps of image treatment.

The first step relies on the tool tip identification. From the ($X = 0$ and $Y = 0$) coordinate (image's bottom left corner), the last pixel of ($X = 0$ and $Y+$) coordinate with a 0 grayscale value is found. The Y value is stored as Y_1. From here, the last pixel of ($X+$ and $Y = Y_1$) coordinate with a 0 grayscale value is reached. The X value is memorized as X_1 and the pixel coordinate (X_1 and Y_1) represents the tool tip position.

From $Y = 0$, each column is analyzed to find the last pixels having 255 grayscale values and ($X > X_1$ and $Y+$) coordinates. Thus, coordinates of the cutting edge are obtained and stored in a matrix named M_1.

Then, a grayscale value from where every grayscale values below will be set to 0 (black) is defined. This value is chosen at the junction of chip surface and the

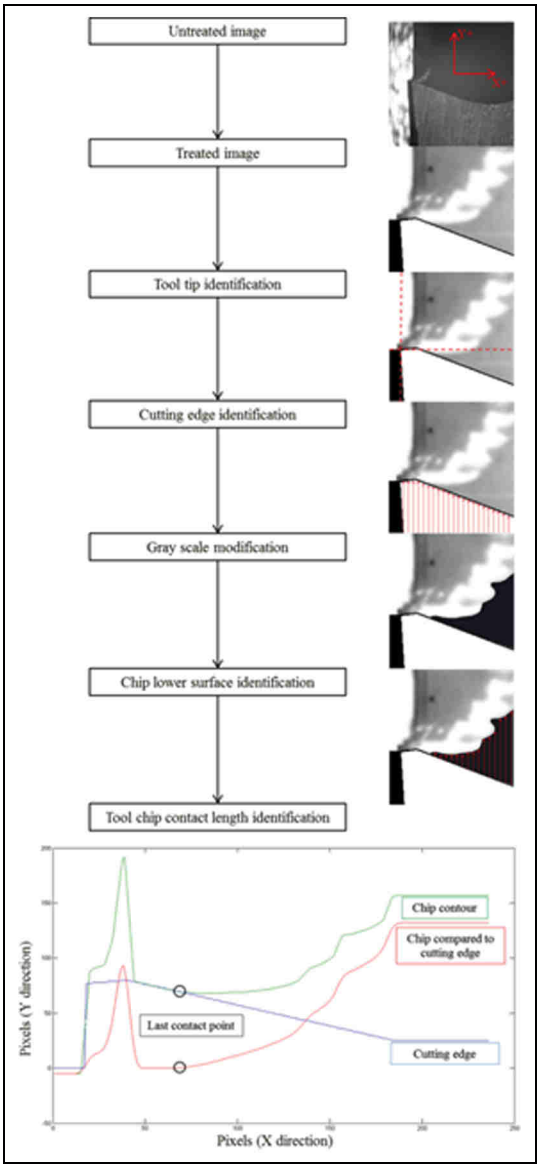

Figure 3. Major steps of image treatment.

image background. From pixels belonging to the cutting edge, the last pixels with 0 grayscale values are sought, column by column, in positive Y direction. These pixel coordinates are gathered in a matrix named M_2.

M_2 and M_1 are compared for each X position and the last point where M_2 value of Y is different from M_1 value of Y gives the last point of tool–chip contact. Knowing this point, the tool–chip contact length is calculated.

Results and discussion

Experimental results

Figures 4 and 5 exhibit tool–chip contact length measurements gathered for each cutting condition (in terms of cutting speeds V_w, feed–chamfer length ratios t_1/b_{cf} and tool–chip contact length–chamfer length ratios L_c/b_{cf}) and tool geometry. Each result sums up measurements made on 100 images of tool–chip contact lengths within cutting process. For a better understanding of the effect of cutting conditions and tool geometry, these results are shown in terms of boxplot and tool–chip contact lengths (L_c) are compared to the chamfer length of the considered tool (b_{cf}). This representation allows taking into account repartition of the values and thus privileged contact length for each stack of data. On these boxplots are represented the 5th centile (the low extremity of the segment), the first quartile (the low part of the box), the median (the mark in the box), the third quartile (the high part of the box) and, finally, the 95th centile (the extremity of the segment). The interpretation of these boxplots can be done this way. Values between the first quartile and the median will represent the range of tool–chip contact lengths considered as the most representative of tool–chip contact lengths during the cutting process (e.g. the most common) for each set of tool geometry and cutting conditions. The area between the median and the third quartile will show the capability of the chip to remain quite stable (small area compared to the one between the first quartile and the median) or to have intense variability during the cutting process (huge area compared to the one between the first quartile and the median). Finally, the area between the third quartile and the 95th centile will exhibit whether the tool–chip contact length often takes really high values or not (respectively, when the area is important or not).

Thus, for each tool and cutting velocity, it can be seen that the general behavior of tool–chip contact lengths (related to the area between the first quartile and the median) will be to increase linearly as the feed increases. Still considering the general behavior, it is seen that going from a cutting speed of 50–80 m min^{-1} will lead to a diminution of the tool–chip contact length in most of the cases for feed–chamfer length ratios of 1 and 2. Cutting speed has no major influence for ratios of 0.5. The chamfer length does not really affect general tool–chip contact lengths. Finally, an increase in rake angle from 10° to 20° will decrease general tool–chip length values (this observation is made with 0.087- and 0.09252-mm chamfer length tools).

Concerning the second area, an important variability of tool–chip contact lengths is generally observed for feed–chamfer length ratios of 2, where it seems ratios of 0.5 and 1 do not show significant impact on this variability. An increase in cutting speed will stabilize values of tool–chip contact lengths for feed–chamfer length ratios of 1. If no impact on variability of the tool–chip contact length is found for rake angles of 20° when increasing the chamfer length, it will stabilize the chip for a rake angle of 10° and feed–chamfer length ratios of 1.

Finally, for the last area between the third quartile and the 95th centile, no general assumption can be made about the influence of feed on the chip capability to often take high values. Nevertheless, this area is

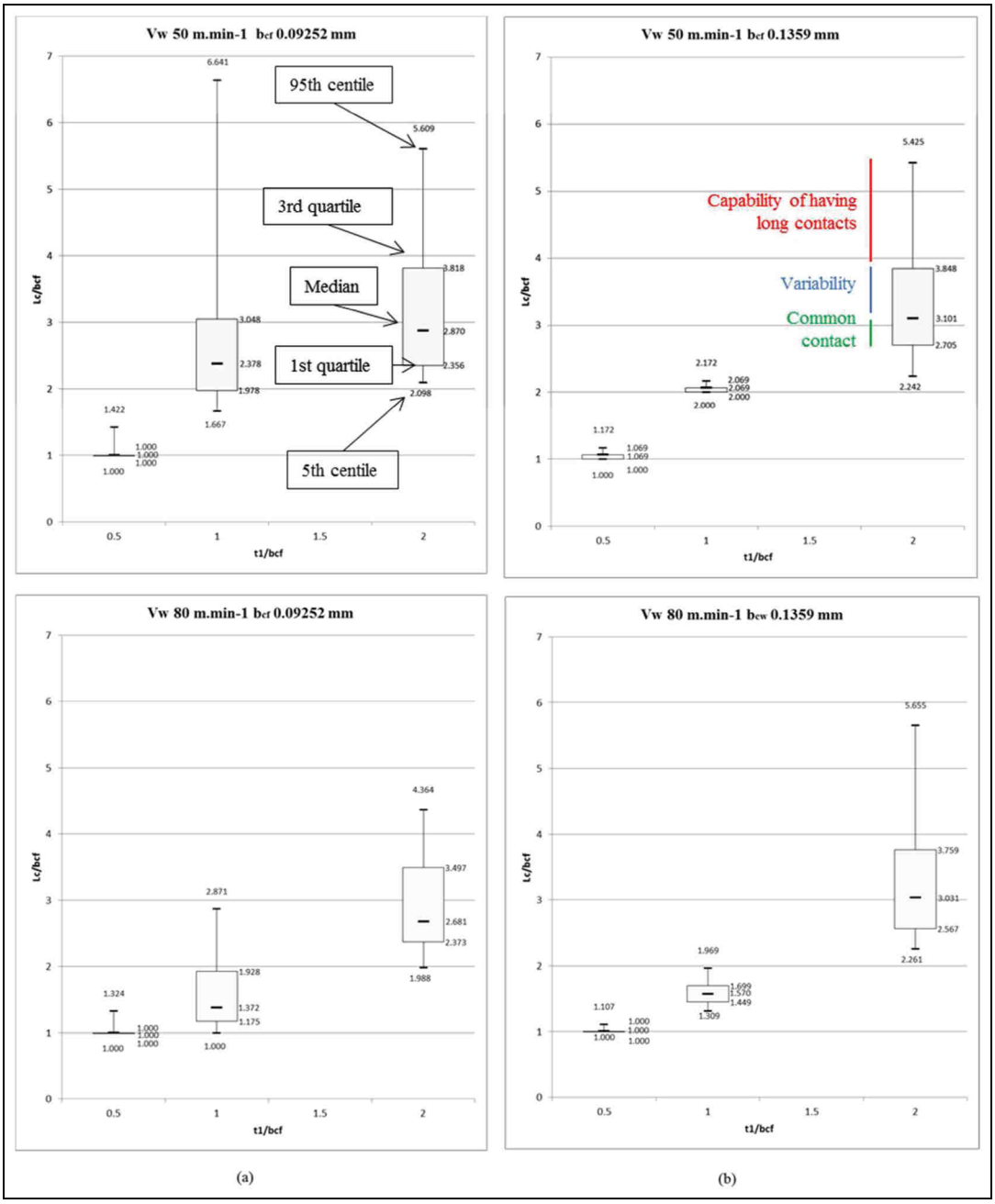

Figure 4. Tool–chip contact length for 10° rake angle tools compared to chamfer length and against feed and cutting speed: (a) chamfer of 0.09252-mm length and (b) chamfer of 0.1359-mm length.

generally pronounced for two feed–chamfer length ratios. Moreover, this area highly depends on the tool geometry and is slightly modified with the cutting speed. Indeed, an increase in cutting speed from 50 to 80 m min^{-1} will make this area reduce.

Discussion

Presentation of the model used

Based on the analytical model of cutting process for chamfered tools developed by Ren and Altintas,[18] the aim is to understand results obtained in the previous section by the analysis of temperatures and apparent friction coefficients. This model is derived from the slip-line model for sharp cutting edge proposed by Hastings et al.[20] The one used in this article assumes that a surface layer of the material with a thickness t_1 flows through the primary shear deformation zone (AB) and separates around a stagnant point B (edge of the dead metal zone) to form the chip with a thickness t_2. A part of the material will flow in the chip and the other part under the flank face of the tool. The chamfer geometry is defined by an angle α_1 and a length b_{cf}. The hypothesis is made that the surface going from the rake face tip H to the stagnation point B will have an angle equal to the main rake angle, for

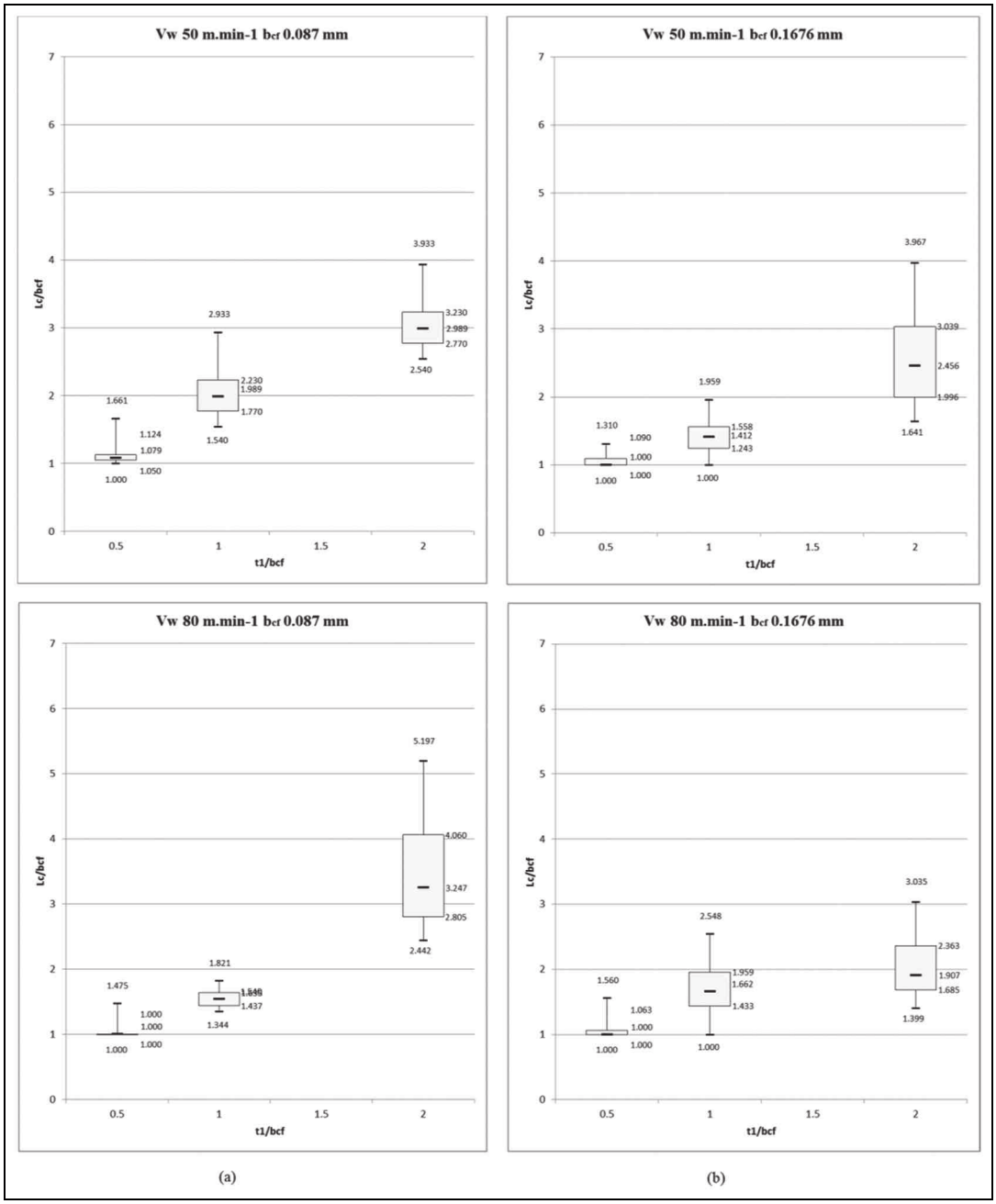

Figure 5. Tool–chip contact length for 20° rake angle tools compared to chamfer length and against feed and cutting speed: (a) chamfer of 0.087-mm length and (b) chamfer of 0.1676-mm length.

example, α_0. As well, the surface heading from the stagnation point B to the tip of the flank face O will have an angle equal to the shear angle ϕ_s. Finally, cutting, shear and chip velocities are, respectively, named V_w, V_s and V_c. The whole geometry of the cutting process is shown in Figure 6.

With the formulation proposed by Oxley,[7] the temperature rise in the primary zone is given by

$$T_{AB} = T_r + \frac{(1-\beta)_{F_s \cos \alpha_0}}{\rho c t_1 w \cos(\phi_s - \alpha_0)} \quad (1)$$

where T_r, ρ and c are the initial temperature, the density and the specific heat of work material, respectively. Dependence of the specific heat with temperature is taken into account in this article. F_s is the shear force and is calculated by the formulation developed by Merchant[21]

$$F_s = F_c \cos \phi_s - F_t \sin \phi_s \quad (2)$$

where F_c and F_t are the forces in cutting direction and feed direction and are measured with the force dynamometer. In this article, the cutting process model for chamfered tools is used in order to find forces contributed by the chamfered zone ($F_{cf\text{-}c}$ and $F_{cf\text{-}t}$).

Knowing these forces will allow getting tangential and normal forces F_{tc} and F_{nc} along the contact

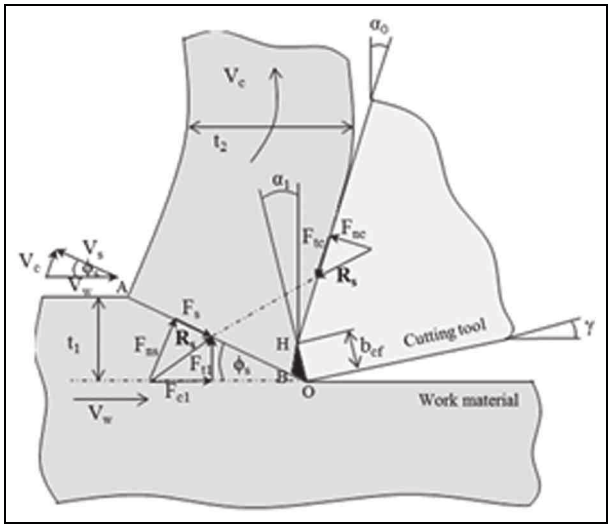

Figure 6. Chip formation model for cutting with chamfered tools.

between the chip and the tool. These forces are given by the following equations

$$\begin{cases} F_{cf-c} = (\tau_{BO}\cos\phi_s + \sigma_{BO}\sin\phi_s)\dfrac{b_{cf}\sin\alpha_1 w}{\cos\phi_s} \\ F_{cf-t} = (\sigma_{BO}\cos\phi_s - \tau_{BO}\sin\phi_s)\dfrac{b_{cf}\sin\alpha_1 w}{\cos\phi_s} \end{cases} \quad (3)$$

where τ_{BO} and σ_{BO} are the tangential and normal stresses developed along the dead metal interface BO. These stresses are given by

$$\begin{cases} \sigma_{BO} = k_{cf}\left(1 + \dfrac{3\pi}{2} - \sin 2\phi_s\right) \\ \tau_{BO} = k_{cf}\cos 2\phi_s \end{cases} \quad (4)$$

$$k_{cf} = \frac{\sigma_{cf}}{\sqrt{3}} \quad (5)$$

with σ_{cf} the flow stress in the chamfer zone which varies with the strain, the strain rate and the temperature by the use of a Johnson Cook law (with parameters suitable for TA6V αβ alloys). Then, tangential and normal forces along the contact between the chip and the tool are

$$\begin{cases} F_{tc} = \left(F_t - F_{cf-t}\right)\cos\alpha_0 + \left(F_c - F_{cf-c}\right)\sin\alpha_0 \\ F_{nc} = \left(F_c - F_{cf-c}\right)\cos\alpha_0 - \left(F_t - F_{cf-t}\right)\sin\alpha_0 \end{cases} \quad (6)$$

and the apparent friction coefficient is

$$\mu = \frac{F_{tc}}{F_{nc}} \quad (7)$$

General behavior of the chip

The apparent friction coefficient will give information about the curl of the chip and thus tool–chip contact lengths as it has been described in previous sections.[22] Results obtained for shear angles (measured on 100 images and averaged), deformed chip thickness t_2, temperature rises in the primary zone and apparent friction coefficient, each tool geometry and cutting conditions are shown in Figures 7 and 8.

First, it is important to say that results obtained with a feed–chamfer length ratio of 0.5 cannot be compared to other results with ratios of 1 and 2. Indeed, for the latter, a dead metal zone is created, putting ourselves in positive rake angle conditions whereas no dead metal zone was formed for ratios of 0.5. In this condition, the chamfer edge acts like the main cutting edge and will cut with a negative angle. Thus, low values of shear angles are found for this condition leading to the highest temperature rises observed in the primary zone. This is due to an increase in plastic work of the shear. These temperatures represent the initial temperature of the chip before it slides on the rake face. Since the friction coefficient is highly dependent on the material temperature (will decrease as the temperature increases), the lowest values of the apparent friction coefficient observed are found for 0.5 ratios. Hence, a huge predominance of the normal force along the contact between the chip and the tool is obtained and the chip will almost have no curvature. This is why the chip will cover the totality of the chamfer length and experiments few contacts on the rake face as it can be seen in Figures 5 and 6. For this ratio, low curves induced by high temperatures in the primary zone are prepondering. Thus, this is the reason why no major influence of cutting speed or tool geometry on tool–chip contact lengths can be found. Indeed, temperature variations created by a change in cutting speed or geometry are too small.

Concerning feed–chamfer length ratios of 1 and 2, it can be seen that an increase in this ratio leads to an increase in shear angle and so a decrease in temperature rises in the primary zone, still because of less plastic work developed. This should lead to an increase in the apparent friction coefficient. However, a decrease is observed. This is mainly due to the fact that for the ratio of 1, most of the friction occurs between the chip and the dead metal zone whereas this specific contact will represent a smallest part of the general contact for the ratio of 2. Moreover, the average friction coefficient between titanium and titanium is higher than the one between tungsten carbide and titanium. This explains the decrease in apparent friction coefficient between ratios of 1 and 2. Then, the chip will have less curvature for ratio of 2 than for ratio of 1 and will exhibit highest tool–chip contact length–chamfer length ratios.

About cutting speeds, in each case, an increase in the cutting speed will increase the shear angle and thus decrease the temperature rise in the primary zone and increase the chip velocity. This effect is more pronounced for tools with a rake angle of 10°. The apparent friction coefficients will increase and so the chip curvature too. Thereby, tool–chip contact length–chamfer length ratios will decrease.

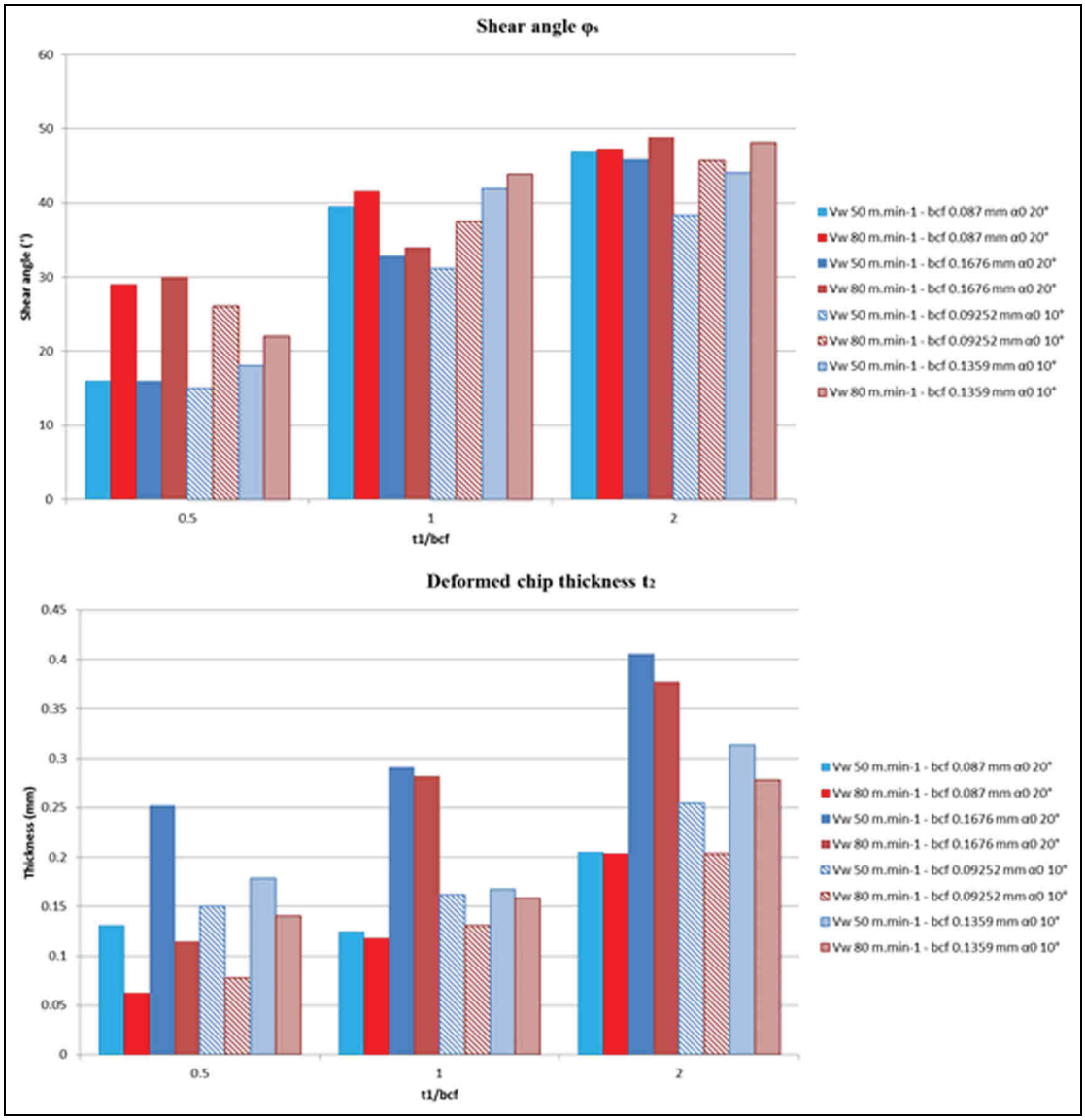

Figure 7. Measured and averaged shear angles ϕ_s and deduced deformed chip thicknesses t_2 for each tool geometry and cutting condition.

The present model cannot help understand the influence of chamfer lengths on tool–chip contact lengths obtained. Indeed, there is an increase in shear angle when the chamfer length increases for 20° rake angles and a decrease for 10° rake angles. Temperatures in the primary zone will inversely follow these results. However, there is no more correlation with these assumptions and apparent friction coefficients observed since they appear to keep steady whatever the chamfer length value takes (except for a cutting speed of 80 m min^{-1}, a chamfer length of 0.1359 and a rake angle of 10°). This might come from the fact that the model does not take into account indentation effects which should not be neglected when increasing the chamfer length.

Finally, by making the comparison between the tool with a chamfer length of 0.087 mm and rake angle of 20° and the one with a chamfer length of 0.092 mm and rake angle of 10°, observations about the effect of rake angle can be made. An increase in rake angle will lead to an increase in shear angle and then a decrease in temperatures in the primary shear zone. Hence, the apparent friction coefficient will decrease, leading chips made with 10° rake angle tools to have less curvature than the one obtained with 20° rake angle tools. Thereby, tool–chip contact length–chamfer ratios will increase as the rake angle decreases.

Variability of the chip

The curvature of the chip will make the chip to have a spiral form and encounter the workpiece. As it can be seen in Figure 9, this will lead the chip to have greater contact length values within a short time, until its breaking appears and a new cycle starts.[23] These instantaneous increases in contact lengths correspond to the

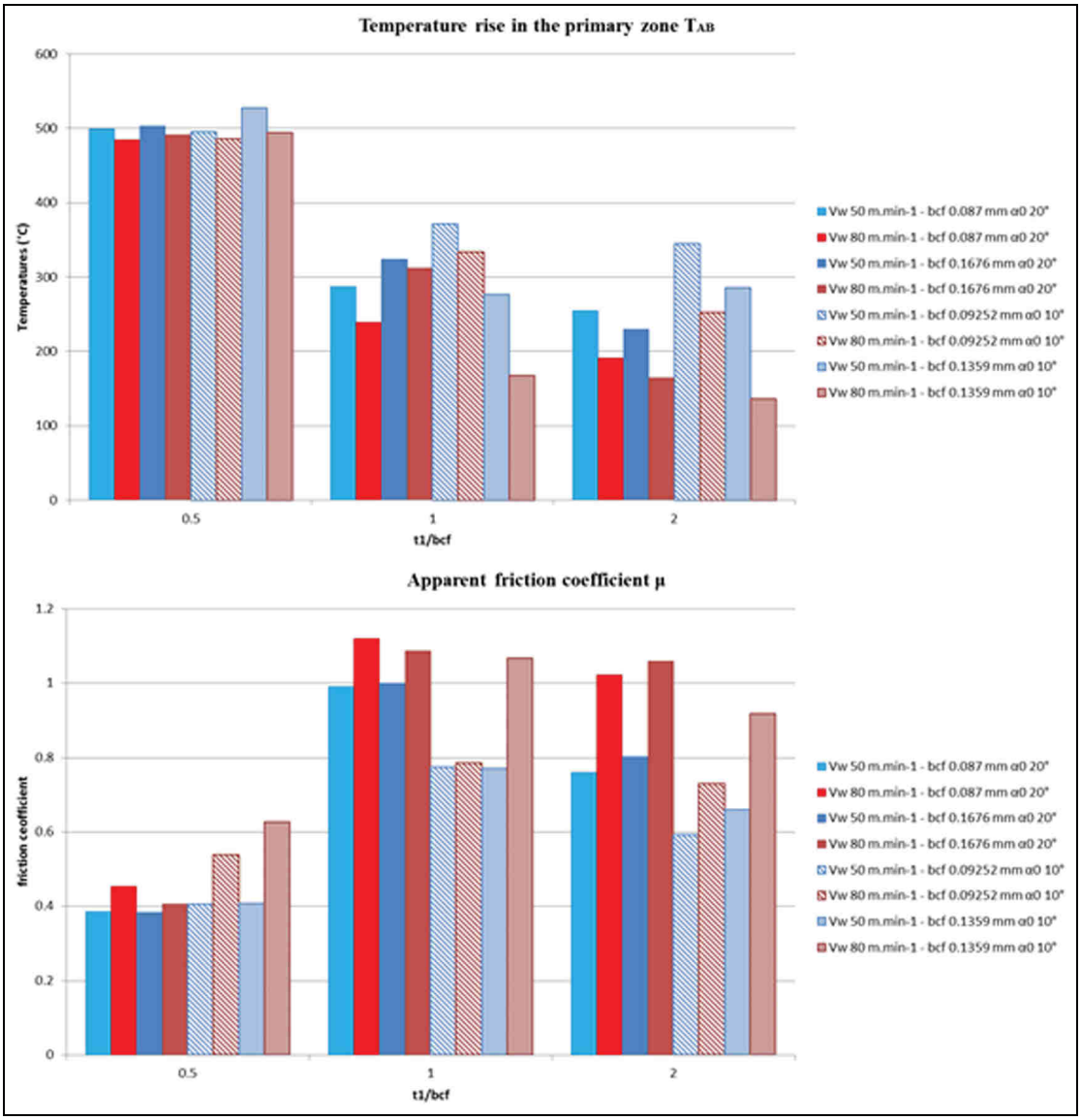

Figure 8. Calculated temperature rises in the primary zone T_{AB} and apparent friction coefficients μ for each tool geometry and cutting condition.

variability of the tool–chip contact length–chamfer length ratio noted in the last section. It is also linked to the capability of the chip to often take high values or not. If the feed–chamfer length ratio will induce the main curvature of the chip, as it has been seen before, cutting velocities, chamfer lengths and rake angles will impose more or less curvature to the initial tendency. Hence, higher curvature will make tool contact lengths to have less variability since the chip can curve more and will less flow on the rake face before breaking appears. From analysis shown before, correlation can be made with results exposed in the previous section. The chip exhibits highest curvature with increasing cutting speeds and rake angles. Thereby, tool–chip contact lengths will show less variability.

Finally, high variabilities and capability of the chip to often reach high values of contact lengths for feed–chamfer length ratios of 2 (independently from cutting speed, rake angle or chamfer length) come from high values of deformed chip thickness in these cases. Indeed, due to higher rigidities induced by these thicknesses, chips will need more stresses in order to break, making them reach higher contact length values before breaking.

From the general behavior of the tool–chip contact length and its variability, the tool will undergo different contact interactions on its rake face. Energy-dispersive X-ray spectroscopy (EDX) observations of two inserts' rake faces have been made in order to understand nature of contacts (Figure 10). These results are for cutting speed of $80\,\mathrm{m\,min^{-1}}$ and a feed–chamfer length ratio of 2. In both cases, three zones can be distinguished. A first zone with almost no titanium deposit and of an equivalent length is really close to the chamfer length. This can be explained by the fact that the chip does not flow on this part due to the presence of

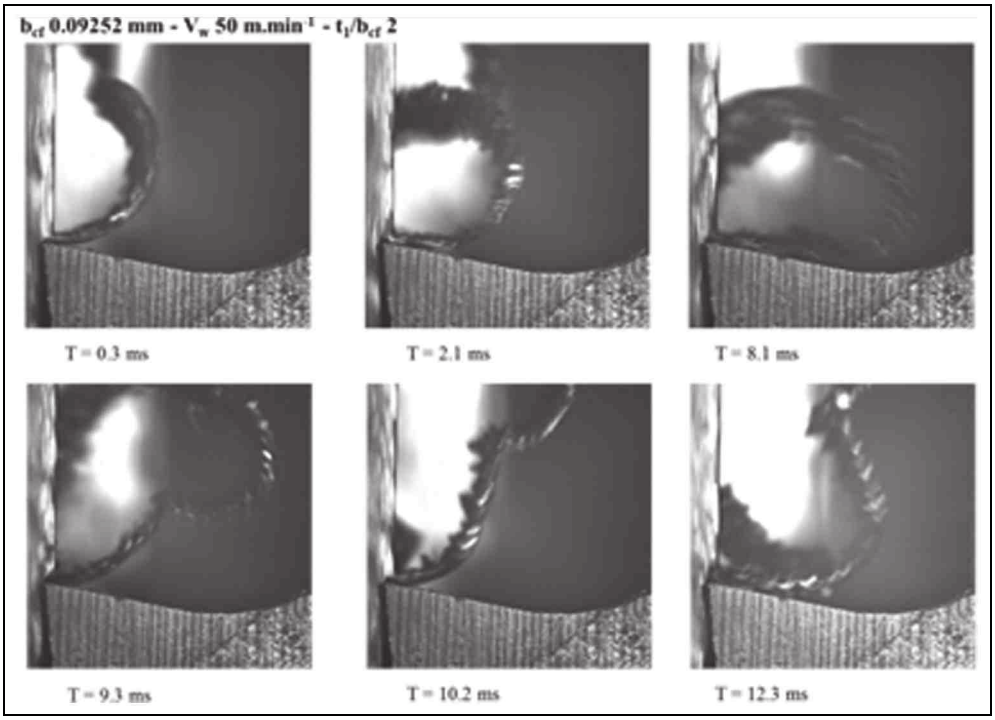

Figure 9. Chip formation according to time: b_{cf}, 0.09252 mm; γ, 20°; V_w, 50 m min^{-1}; and t_1/b_{ch}, 2.

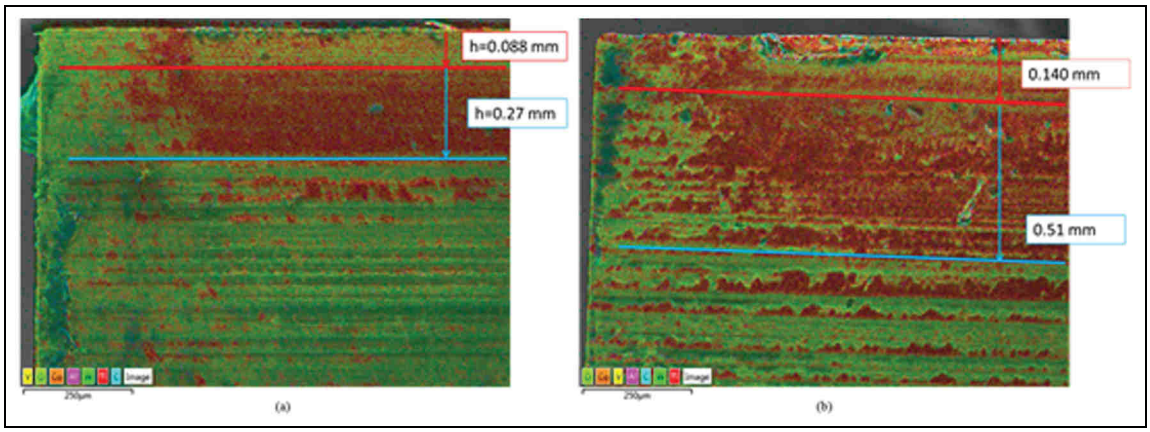

Figure 10. EDX observations of cutting tools: (a) b_{cf}, 0.09252; γ, 10°; t_1/b_{ch}, 2; and V_w, 80 m min^{-1} and (b) b_{cf}, 0.1359; γ, 10°; t_1/b_{ch}, 2; and V_w, 80 m min^{-1}.

the dead metal zone. The second part with a massive deposit of titanium has a length located between the first and the third quartiles. This large presence of titanium shows the tool underwent high pressure and temperature contacts, enough for the titanium to diffuse in it. This can be related to the general behavior of the contact length discussed before. Then, a third part exhibits little titanium deposit and almost reaches upper values of the tool–chip contact length. This part would be the result of the variability of the tool–chip contact length. In this part, pressures and temperatures are less important. Indeed, pressures will be the consequence of contacts between the chip and the workpiece. As it can be seen on EDX images, these pressures are not enough to make the deposit of titanium cover striation hollows.

Zorev[24] friction model between the chip and the rake angle is the most used in cutting models. In this model, the normal stress takes its higher value at the tool tip and then gradually decreases to zero at the end of the contact length. The frictional shearing stress will have two zones, the first called sticking friction followed by the second defined as the sliding friction.

In the sticking friction, the frictional shearing stress is equal to average shear flow stress at tool interface. In sliding friction, the shear stress will decrease the same way as the normal stress (with a friction coefficient) from this value to zero. Sticking and sliding contact lengths are usually found by observations of the rake face wear of tools. The zone with high deposit of titanium is considered as the sticking contact whereas the

zone with almost no titanium deposit is considered as the sliding friction. From the prior analysis in this article, it is obvious that considering only tool wear observations will induce an overestimation of pressure and shearing stresses in the sliding friction. Indeed, the sliding friction is not steady during cutting process.

Conclusion

This article has presented a tool–chip contact length analysis of orthogonal cutting of a TA6V αβ with chamfered tools of various geometries and with several cutting conditions. This analysis has been based on cutting force measurements as well as image analysis obtained at high-speed frequency during the cutting process. Based on a model of cutting process with chamfered tools,[18] it has been shown that

- Cutting with a feed–chamfer length ratio of 0.5 will make the chip to flow parallel to the chamfer edge and have few curvature. Thus, the chip will cover the totality of the chamfer edge and will not often flow on the rake face. This assumption is regardless of the cutting speed, rake angle or chamfer length.
- Beyond feed–chamfer length ratios of 1, the tool–chip contact length–chamfer length ratio will increase with feed–chamfer length ratios. This is mainly due to the percentile of friction that will occur between the chip and the dead metal zone compared to the friction with the chip and the rake face. Friction coefficients are higher between titanium and titanium than between titanium and tungsten carbide. Thereby, an increase in feed–chamfer length ratios will decrease the curvature of the chip and generate higher contact surfaces between the chip and the rake face.
- An increase in cutting speed will increase shear angles and then reduce temperatures along the shear primary zone (due to less plastic work). Since friction coefficients decrease with temperature, the chip will exhibit more curvature and lead to smaller tool–chip contact length–chamfer length ratios. Moreover, chip curvatures make possible the apparition of contacts between the chip and the workpiece. This led the tool–chip contact length to grow before breaking of the chip appears. When curvatures are more important, the capability of the chip to curve easily makes these extended contacts smaller. Then, an increase in cutting speed will also stabilize tool -chip contact lengths, for example, variations of tool -chip contact lengths will be smaller and the chip will less encountered really high tool -chip contact lengths.
- The same assumption can be made with an increase in rake angle.
- There is no effect of the cutting speed and rake angle on this variation for feed–chamfer length ratio of 2 because of high deformed chip thickness (for this ratio), and the chip will have more rigidity and break less easily, leading to high variabilities of contact lengths.

EDX analysis has shown that these variabilities are the main reason of various interaction surfaces usually observed on tool's rake faces. Indeed, sticking friction zones generally observed are directly related to the general behavior of tool–chip contact lengths induced by the feed. However, the sliding friction area is due to tool–chip contact length variabilities imposed by cutting velocities and rake angles. The sliding friction zone is taken steady in most of pressure and shear stress models at tool–chip interface. Since the sliding friction area is variable during cutting process, these models might lead to an overestimation of normal and shear stresses on the rake face.

Declaration of conflicting interests

The author(s) declared no potential conflicts of interest with respect to the research, authorship and/or publication of this article.

Funding

The author(s) disclosed receipt of the following financial support for the research, authorship, and/or publication of this article: This work was conducted under the "Titanium Machining and Simulation" project, funded by the Midi-Pyrenees region and the French state under agreement FUI APP12–TIMAS together with various manufacturers (Airbus Saint-Eloi, Figeac Aero, Aubert & Duval, Impetus and Aurock) and research laboratories (LGP Tarbes, ICA Toulouse and Bordeaux I2M).

References

1. Wagner V and Duc E. Study of Ti-1023 milling with toroidal tool. *Int J Adv Manuf Tech* 2014; 75: 1473–1491.
2. Wagner V, Baili M and Dessein G. The relation between the cutting speed, tool wear and chip formation during Ti-5553 dry cutting. *Int J Adv Manuf Tech* 2015; 76: 893–912.
3. Zorev NN. *Metal cutting mechanics*. Oxford: Pergamon Press, 1966.
4. Lee EH and Shaffer W. The theory of plasticity applied to the problem of machining. *J Appl Mech: T ASME* 1951; 18: 405–413.
5. Abuladze NG. Character and the length of tool-chip contact (in Russian). In: *Proceedings of the machinability of heat-resistant and titanium alloys*, Kuibyshev, 1962, pp.68–78.
6. Zhang HT, Liu PD and Hu RS. A three zone model and solution of shear angle in orthogonal machining. *Wear* 1991; 143: 29–43.
7. Oxley PLB. *Mechanics of machining: an analytical approach to assessing machinability*. Chichester: Ellis Horwood Limited, 1989.

8. Lazoglu I and Altintas Y. Prediction of tool and chip temperature in continuous and interrupted machining. *Int J Mach Tool Manu* 2002; 42: 1011–1022.
9. Armarego EJA. *Material removal processes—an intermediate course*. Melbourne, VIC, Australia: University of Melbourne, 1993.
10. Moufki A, Molinari A and Dudzinski D. Modelling of orthogonal cutting with a temperature dependent friction law. *J Mech Phys Solids* 1998; 46(10): 2103–2138.
11. Movahhedy MR, Gadala MS and Altintas Y. Simulation of the orthogonal metal cutting process using an arbitrary Lagrangian-Eulerian finite element method. *J Mater Process Tech* 2000; 103: 267–275.
12. Lin ZC and Lin SY. A coupled finite element model of thermo-elastic-plastic large deformation for orthogonal cutting. *J Eng Mater: T ASME* 1996; 118: 545–554.
13. Calamaz M, Coupard D, Nouari M, et al. A finite element model of high speed machining of TA6V titanium alloy. In: *Proceedings of 6th international conference high speed machining*, San Sebastian, Spain, March 2007, pp.21–22.
14. Movahhedy MR, Altintas Y and Gadala MS. Numerical analysis of metal cutting with chamfered and blunt tools. *J Manuf Sci E: T ASME* 2002; 124: 178–188.
15. Sun S, Brandt M and Dargusch MS. Effect of tool wear on chip formation during dry machining of Ti-6Al-4V alloy, part I: effect of gradual tool wear evolution. *Proc IMechE, Part B: J Engineering Manufacture*. Epub ahead of print 3 September 2015. DOI: 10.1177/0954405415599956.
16. Sun S, Brandt M and Dargusch MS. Effect of tool wear on chip formation during dry machining of Ti-6Al-4V alloy, part II: effect of tool failure modes. *Proc IMechE, Part B: J Engineering Manufacture*. Epub ahead of print 4 September 2015. DOI: 10.1177/0954405415600011.
17. Özel T and Ulutan T. Effects of machining parameters and tool geometry on serrated chip formation, specific forces and energies in orthogonal cutting of nickel-based super alloy Inconel 100. *Proc IMechE, Part B: J Engineering Manufacture* 2014; 228(7): 673–686.
18. Ren H and Altintas Y. Mechanics of machining with chamfered tools. *J Manuf Sci E: T ASME* 2000; 122: 650–659.
19. Rasband WS. *ImageJ*. Bethesda, MD: US National Institutes of Health, http://imagej.nih.gov/ij/ (1997, accessed 2014).
20. Hastings WF, Mathew P and Oxley PLB. A machining theory for predicting chip geometry, cutting forces, etc. from work material properties and cutting conditions. *P Roy Soc Lond A Mat* 1980; 371: 569–587.
21. Merchant ME. Basic mechanics of the metal cutting process. *J Appl Mech* 1944; 11: 168–175.
22. Friedman MY and Lenz E. Investigation of the tool-chip contact length in metal cutting. *Int J Mach Tool D R* 1970; 10: 401–416.
23. Jawahir IS and Van Luttervelt CA. Recent developments in chip control research and applications. *CIRP Ann Manuf Technol* 1993; 42(2): 659–693.
24. Zorev NN. Inter-relationship between shear processes occurring along tool face and shear plane in metal cutting. In: *Proceedings of the international research in production engineering*, Pittsburgh, PA, 9–12 September 1963, pp.42–49. New York: ASME.

Appendix I

Notation

b_{cf}	chamfer length
c	specific heat
F_c and F_t	forces in cutting and feed directions
$F_{cf\text{-}c}$ and $F_{cf\text{-}t}$	forces contributed by the chamfered zone in cutting and feed directions
F_s	shear force
F_{tc} and F_{nc}	tangential and normal forces along the contact between the chip and the tool
L_c	tool–chip contact length
t_1	feed
t_2	chip thickness
T_{ab}	average rise of temperature in the primary shear zone
T_r	initial temperature
V_c, V_s and V_w	chip, shear and cutting speeds
α_0 and α_1	rake and chamfer angles
β	fraction of heat going through the workpiece
μ	apparent friction coefficient
ρ	density
σ_{BO} and τ_{BO}	normal and tangential stresses developed along the dead metal interface *BO*
σ_{cf}	flow stress in the chamfer zone
ϕ_s	shear angle